Chemical Science

ROYAL SOCIETY OF CHEMISTRY

EDGE ARTICLE

View Article Online
View Journal | View Issue

Check for updates

Cite this: *Chem. Sci.*, 2024, **15**, 10945

All publication charges for this article have been paid for by the Royal Society of Chemistry

Self-assembly-integrated tumor targeting and electron transfer programming towards boosting tumor type I photodynamic therapy†

Wenlong Chen,‡[ab] Zehui Wang,‡[b] Gaobo Hong,[b] Jianjun Du,[b] Fengling Song *[ab] and Xiaojun Peng[b]

Type I photodynamic therapy (PDT) is attracting increasing interest as an effective solution to the poor prognosis of patients with hypoxic tumors. The development of functional type I photosensitizers is limited by a lack of feasible strategies to systematically modulate electron transfer (ET) in photosensitization. Herein, we present an easily accessible approach for the preparation of nanophotosensitizers with self-assembly-integrated tumor-targeting and ET programming towards boosting tumor type I PDT. Specifically, a dual functional amphiphile **PS-02** was designed with a ligand (**6-NS**) that had the ability to not only target tumor cell marker carbonic anhydrase IX (**CAIX**) but also regulate the ET process for type I PDT. The amphiphile **PS-02** tended to self-assemble into **PS-02** nanoparticles (NPs), which exhibited a local "ET-cage effect" due to the electron-deficient nature of **6-NS**. It is noteworthy that when **PS-02** NPs selectively targeted the tumor cells, the **CAIX** binding enabled the uncaging of the inhibited ET process owing to the electron-rich characteristic of **CAIX**. Therefore, **PS-02** NPs integrated tumor targeting and **CAIX** activation towards boosting type I PDT. As a proof of concept, the improved PDT performance of **PS-02** NPs was demonstrated with tumor cells under hypoxic conditions and solid tumor tissue in mouse *in vivo* experiments. This work provides a practical paradigm to develop versatile type I PDT nano-photosensitizers by simply manipulating ET and easy self-assembling.

Received 7th May 2024
Accepted 5th June 2024

DOI: 10.1039/d4sc03008g

rsc.li/chemical-science

Open Access Article. Published on 18 June 2024. Downloaded on 1/21/2026 10:49:51 PM. This article is licensed under a Creative Commons Attribution-NonCommercial 3.0 Unported Licence.

Introduction

Photodynamic therapy (PDT) for tumor treatment has drawn considerable attention for its merits of non-invasiveness, high cure rate, and minimal side effects compared to chemotherapy, surgery, and radiotherapy.[1,2] Although tumor PDT has made lots of progress in clinical trials and application,[3–6] the full promise of PDT in these merits has not yet been realized in practice. It is revealed that the complex tumor biological environment, for example, abnormal vasculature and tumor heterogeneity, compromises PDT efficiency.[7,8] These unfavorable factors in tumors not only create barriers to the effective delivery of photosensitizer (PS) reagents but also cause the hypoxic environment in tumors.[9–13] In terms of tumor PDT, the effective tumor enrichment of PSs is the first prerequisite,[14] because increasing tumor PS enrichment can reduce the toxic side effects on normal tissues by cutting down the amounts of PSs injected or the intake of normal tissues.[15,16] Besides, it is well known that the hypoxic environment of the tumor directly limits the efficacy of PDT.[1,17–20] This is because most of the photosensitizers (PSs) proved in clinical trials are based on the type II PDT mechanism by sensitizing O_2 to produce singlet oxygen ($^1O_2$). And type II PSs are severely dependent on the O_2 supplement. In order to achieve the desired therapeutic outcomes, advanced PDT treatment protocols call for a combination of tumor targeting and circumvention hypoxic treatment modalities.

Further studies have found that type I PDT, in which PSs could sensitize O_2 to mainly produce the superoxide anion ($O_2^{\bullet-}$), was less oxygen-dependent. It was praised for performing well in the treatment of hypoxic tumors.[3,21–25] So far, several organic PSs, for example, triarylmethanes,[26] benzophenothiazine derivatives,[21] 1,8-naphthalimide-dialkyl-triphenylamine[27,28] and aggregation-induced emission luminogens,[29,30] have been reported to follow the type I PDT mechanism. However, the rational molecular design of novel type I PSs is still in its infancy.[31,32] Considering electron transfer (ET) as the core photophysical process of type I photosensitization, it is believed that the electron-rich environment around PSs could

[a]*Shenzhen Research Institute of Shandong University, A301 Virtual University Park in South District of Shenzhen, 518057, P. R. China. E-mail: songfl@sdu.edu.cn; songfl@dlut.edu.cn*

[b]*State Key Laboratory of Fine Chemicals, Frontiers Science Center for Smart Materials Oriented Chemical Engineering, Dalian University of Technology, Dalian 116024, P. R. China*

† Electronic supplementary information (ESI) available. See DOI: https://doi.org/10.1039/d4sc03008g

‡ Wenlong Chen and Zehui Wang contributed equally to this work.

© 2024 The Author(s). Published by the Royal Society of Chemistry

Open Access Article. Published on 18 June 2024. Downloaded on 1/21/2026 10:49:51 PM.
This article is licensed under a Creative Commons Attribution-NonCommercial 3.0 Unported Licence.

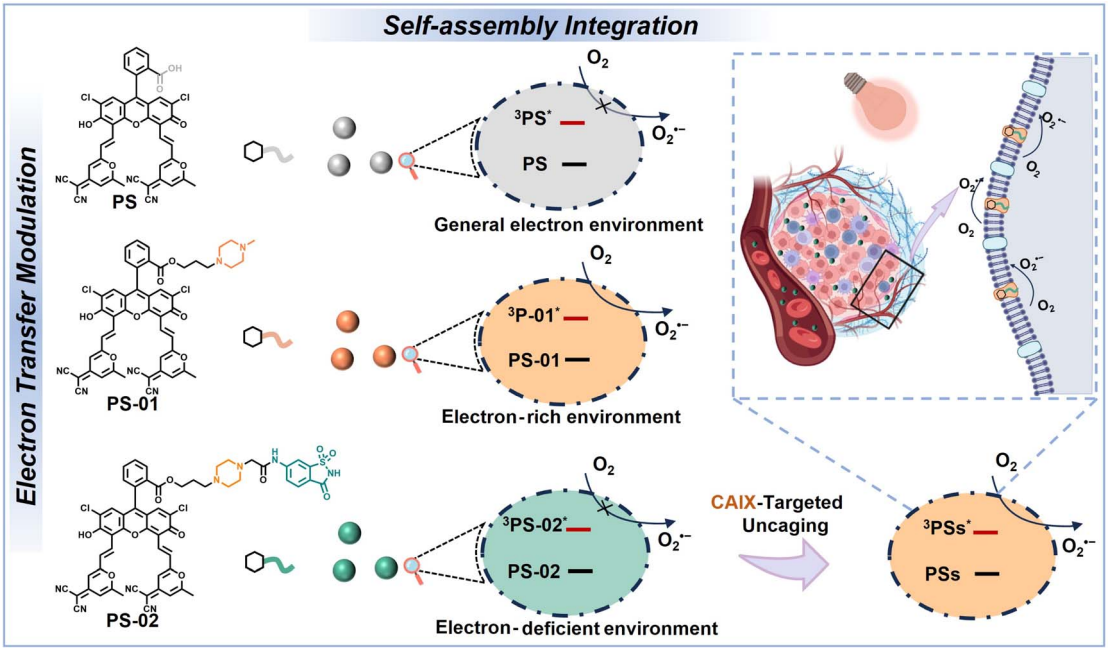

Scheme 1 A brief illustration of the scheme of chemically modifying the structure of amphiphiles' functional molecules and the related self-assembly for nanoparticles.

significantly enhance the ET-based type I process. Following this idea, some traditional type II PSs could transform into dominant type I processes in the electron-rich substrate environment.[33–36] Despite these exciting advances, the therapeutic performance of these type I PDT processes still needed to be improved. For example, these previously reported type I nanophotosensitizers mainly relied on the passive targeting of nanoparticles (enhanced permeability and retention (EPR) effect). The enrichment of the drug in the tumor area remained unsatisfactory. To enable a better PS delivery, tumor-selective antibody or ligand modification and tumor-associated factor activation functionalization have been proposed.[37,38] But until now, these active targeting techniques were rarely fully employed in these previous type I nanophotosensitizers. It is desirable to design versatile PSs which integrate the enhancement of type I PDT with the endowment of tumor targeting.

Recently, amphiphilic molecule self-assembly has drawn great interest in nanomedicine preparation because it provides a facile and "bottom-up" method to manipulate therapeutic building blocks at a molecular level.[39,40] In this work, by rationally tailoring amphiphilic small molecules, self-assembly was leveraged to the bespoke production of nanophotosensitizers with both tumor cell targeting and type I PDT enhancement (Scheme 1). In detail, we have designed and synthesized two amphiphilic small molecules **PS-01** and **PS-02** from a thermally activated delayed fluorescence (TADF) characteristic photosensitizer molecule **PS** developed earlier in our laboratory.[35,41] In the aqueous environment, **PS**, **PS-01**, and **PS-02** could self-assemble into nanoparticles **PS** NPs, **PS-01** NPs, and **PS-02** NPs, respectively. In **PS-01**, the piperazine unit was covalently attached to the **PS** as an electron donor group to provide the local "electron-rich environments" in self-assembled nanoparticles for boosting the type I process. In **PS-02**, a tumor biomarker carbonic anhydrase IX (**CAIX**)-targeting ligand saccharin derivative (**6-NS**) was further modified to the piperazine unit for two purposes. First, by targeting **CAIX**, **PS-02** NPs can achieve tumor-targeting recognition and enrichment.[42,43] **CAIX** is known to be an overexpressed membrane protein in most aggressive forms of cancer such as in cancer stem cells.[44] And the **CAIX**-targeting approach could improve and advance the tumor therapeutic treatments.[45–47] Second, we assumed that the electron-deficient nature of **6-NS** enabled the weakening of the electron donor effect provided by piperazine and turned off the "electron-rich environments" unit by forming an "electron transfer cage" in **PS-02** NPs. When **PS-02** NPs were targeted to tumors, electron-rich **CAIX** could uncage the electron transfer for the type I process. Therefore, **PS-02** NPs could achieve the integration functions of tumor targeting and type I photosensitization enhancement. As a proof of concept, we have proved the feasibility of this design by photosensitization in solution and detected by nanosecond transient absorption that the ET process occurred in the excited state of **PS-01** NPs but not in **PS** NPs and **PS-02** NPs. Meaningfully, **PS-02** NPs were devised to effectively cure tumor cells *in vitro* under hypoxia and tumor tissues in mice *in vivo*. This strategy of self-assembly-integrated tumor targeting and electron transfer programming should become a universal protocol towards boosting tumor type I PDT.

Results and discussion

Molecular synthesis and self-assembly

PS-01 and **PS-02** were synthesized by two steps of substitution reaction (Scheme S1†). First, **PS** and 1,3-dibromopropane were connected by nucleophilic substitution reaction to produce the intermediate **PS-Br**. Then, **PS-Br** underwent a second substitution reaction with *N*-methyl piperazine or the saccharin

© 2024 The Author(s). Published by the Royal Society of Chemistry

Open Access Article. Published on 18 June 2024. Downloaded on 1/21/2026 10:49:51 PM. This article is licensed under a Creative Commons Attribution-NonCommercial 3.0 Unported Licence.

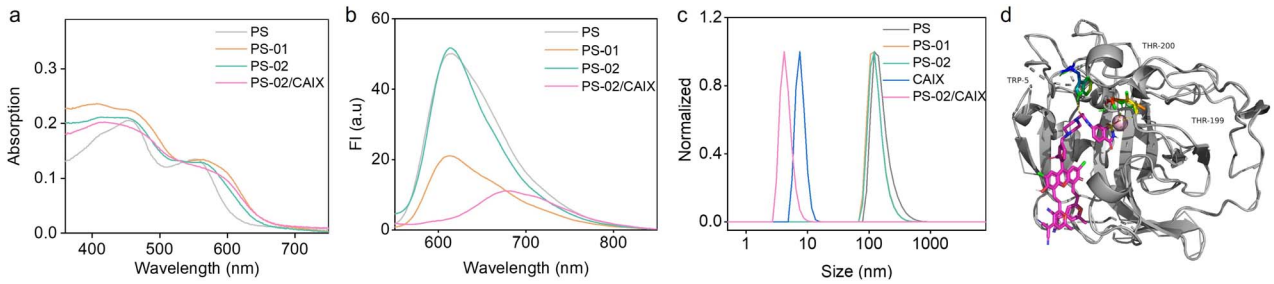

Fig. 1 The basic steady-state spectral properties and self-assembly evaluation in aqueous solutions. (a) The UV-Vis absorption spectra of **PS**, **PS-01**, **PS-02**, and **PS-02/CAIX** (10 μM) in aqueous solution. (b) The fluorescence emission spectra of **PS**, **PS-01**, **PS-02**, and **PS-02/CAIX** (10 μM) in aqueous solution. (c) The **PS**, **PS-01**, **PS-02**, and **PS-02/CAIX** (10 μM) hydrodynamic particle size measured by DLS in aqueous solution. (d) AUTODOCK simulations of binding sites of **PS-02/CAIX** (PDB code: 3IAI).

derivatives (**6-NS**) to obtain the product **PS-01** or **PS-02**, respectively. The specific synthesis process and molecular structure characterization are documented in the ESI.†

The amphiphilic molecular structure of **PS**, **PS-01**, and **PS-02** could endow them with the ability to self-assemble into nanoparticles in the aqueous environment.[48] The UV-Vis absorption spectra of the amphiphiles in an aqueous solution showed no obvious characteristic peak compared with those in an organic solvent (Fig. 1a and S1†). This indicated that self-assembly may occur in the aqueous solution.[49,50] At the same time, the fluorescence intensity of these amphiphiles in the aqueous solution was significantly different (Fig. 1b). **PS-01** decreased to 43% of **PS** in relative fluorescence quantum efficiency, which was consistent with the electron transfer quenching process from the electron donor piperazine (Table S1†). In contrast, **PS-02** exhibited a restored fluorescence quantum efficiency comparable to that of **PS**. From the molecular design, the electron-deficient ligand **6-NS** was expected to work as an "ET cage" to weaken the electron-donor effect of piperazine. So, the electron transfer process of piperazine in **PS-02** should be inhibited to some extent. Furthermore, when **CAIX** was added, the fluorescence intensity of **PS-02** decreased again. This may be explained by the fact that the electron-rich characteristics of **CAIX** could uncage the "electron transfer cage" by forming the **PS-02/CAIX** complex. The transmission electron microscope (TEM) and dynamic light scattering (DLS) experiments were conducted to prove the formation of nanoparticles by self-assembly. **PS** NPs, **PS-01** NPs, and **PS-02** NPs had a spherical structure with an average hydrodynamic size of around 150 nm (Fig. 1c and S2†). Moreover, from the hydrodynamic size change of **PS-02** NPs after adding **CAIX**, we inferred that it should effectively disassemble in the presence of **CAIX**. To verify this,

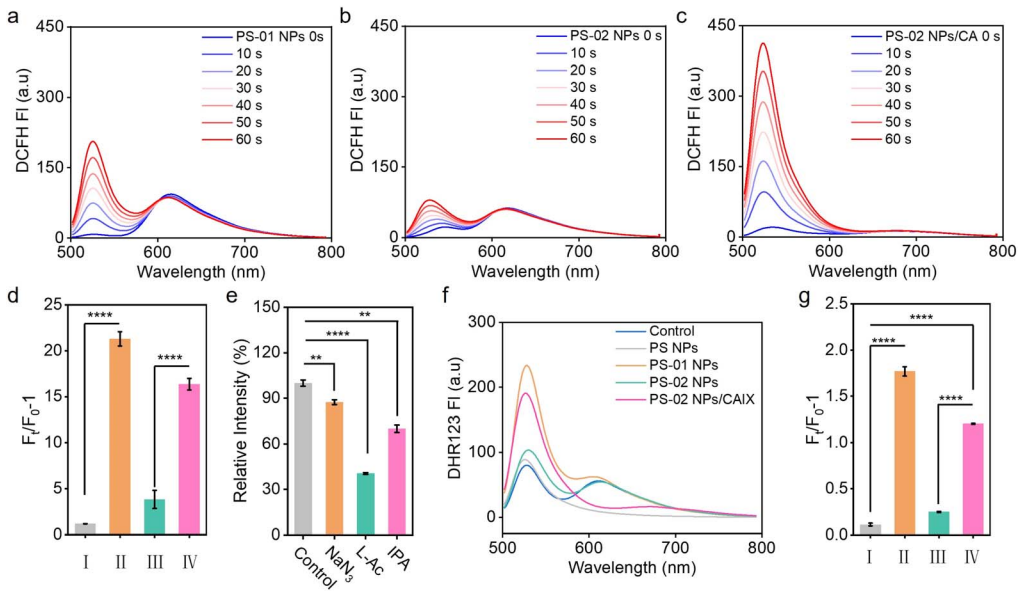

Fig. 2 The photosensitization evaluation in aqueous solutions. General ROS detection by using DCFH (5 μM) for **PS-01** NPs (a), **PS-02** NPs (b) and **PS-02** NPs/**CAIX** (10 μM) (c). (d) The histogram of relative fluorescence intensity of DCFH of **PS** NPs (I), **PS-01** NPs (II), **PS-02** NPs (III), and **PS-02** NPs/**CAIX** (IV) separately after 60 s of irradiation (white light, 2 mW cm^{-2}). (e) The histogram of the normalized relative integration fluorescence intensity ratio of DCFH in the presence of different ROS scavengers for **PS-02** NPs/**CAIX**. (f) The curve graph of relative fluorescence intensity of DHR 123 in **PS** NPs, **PS-01** NPs, **PS-02** NPs and **PS-02** NPs/**CAIX** aqueous solution after light irradiation. (g) The histogram of relative fluorescence intensity of DHR 123 of **PS** NPs (I), **PS-01** NPs (II), **PS-02** NPs (III), and **PS-02** NPs/**CAIX** (IV) separately after irradiation (white light, 2 mW cm^{-2}). Statistical significance was analyzed by the Student's *t*-test. ****$p < 0.0001$; **$p < 0.01$.

Open Access Article. Published on 18 June 2024. Downloaded on 1/21/2026 10:49:51 PM.
This article is licensed under a Creative Commons Attribution-NonCommercial 3.0 Unported Licence.

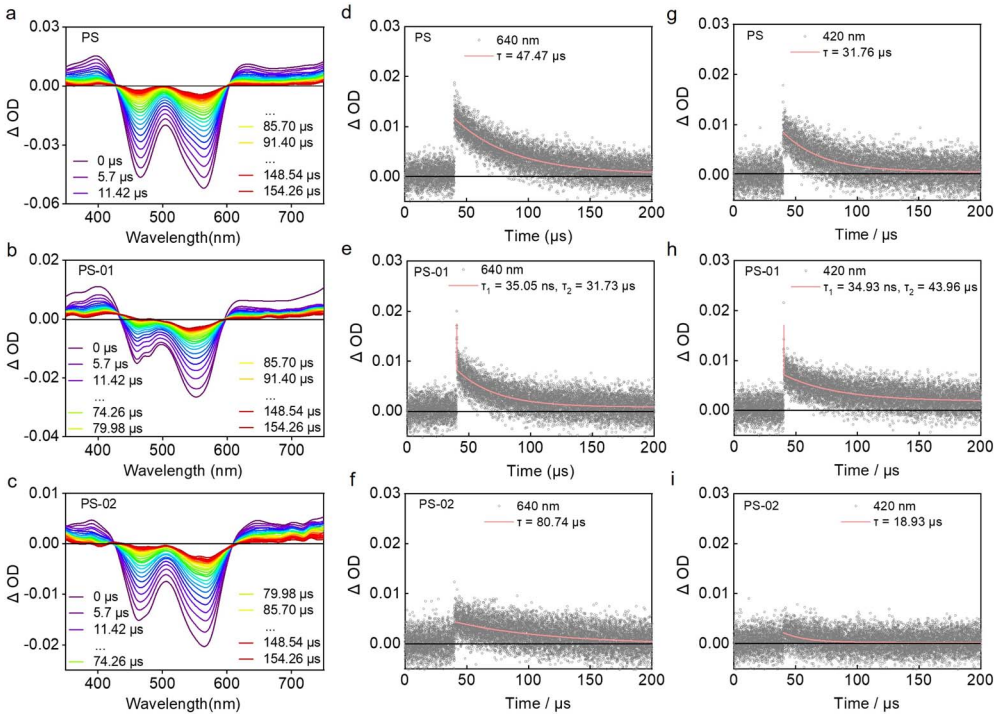

Fig. 3 The transient species and kinetic characterization by nanosecond transient absorption spectroscopy. Time-resolved transient absorption spectra of **PS** NPs (a), **PS-02** NPs (b), and **PS-02** NPs (c) (10 μM) in anaerobic aqueous solutions by nitrogen bubbling. The decay curve at the absorption wavelength of 640 nm of **PS** NPs (d), **PS-02** NPs (e), and **PS-02** NPs (f) (10 μM) in anaerobic aqueous solutions by nitrogen bubbling. The decay curve at the absorption wavelength of 420 nm of **PS** NPs (g), **PS-01** NPs (h), and **PS-02** NPs (i) (10 μM) in anaerobic aqueous solutions by nitrogen bubbling. All samples were excited with a nanosecond pulsed laser, $\lambda_{ex} = 532$ nm.

we performed molecular docking simulation calculations. It can be seen that the **6-NS** ligand group part of **PS-02** could enter into the pocket of **CAIX** and bring about a tight binding effect with a free energy of binding of -4.35 kcal mol^{-1} (Fig. 1d). These results indicate that these amphiphiles could self-assemble into functional NPs.

CAIX-activated photosensitization for boosted $O_2^{\bullet-}$ generation

Next, we investigated whether the binding effect between **CAIX** and **PS-02** could regulate the type I photosensitization process. We tested the photosensitization ability of **PS** NPs, **PS-01** NPs, and **PS-02** NPs in aqueous solutions. The results indicated that **PS-01** NPs had 18.0 times larger ROS amounts than **PS** NPs (Fig. 2a and d). Meanwhile, compared with **PS-01** NPs, **PS-02** NPs showed significantly reduced ROS amounts which were 20% that of **PS-01** NPs (Fig. 2b and d). Importantly, when **CAIX** was added, it could recover the ability of ROS generation (Fig. 2c and d). In order to make clear the **CAIX** effect in ROS generation capacity, we analyzed the ROS components by a single ROS species quenching experiment using specific ROS scavengers NaN_3 (for $^1O_2$),[51] vitamin C (for $O_2^{\bullet-}$)[21] and isopropyl alcohol (for $OH^{\bullet}$)[52] (Fig. 2e). This suggests that $O_2^{\bullet-}$ dominated the ROS generated in the **PS-02** NPs/**CAIX** system. This explained that **CAIX** mainly affects the type I photosensitization process. To confirm this result, another indicator, dihydrorhodamine 123 (DHR 123), was used for confirming $O_2^{\bullet-}$ generation. As can be

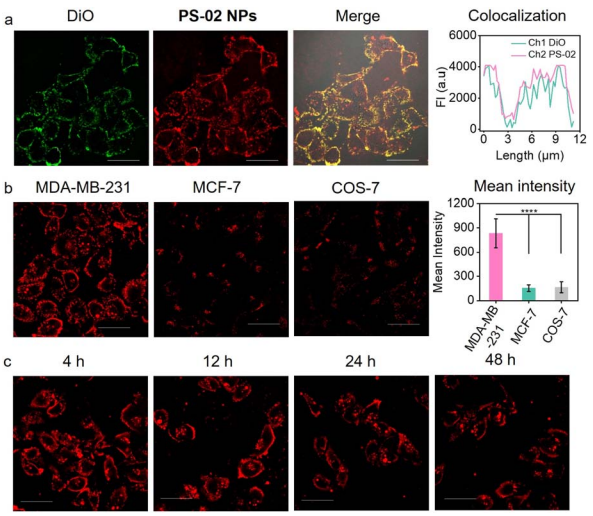

Fig. 4 Photosensitizer staining assessment of live cells. (a) Cell membrane colocalization CLSM imaging of MDA-MB-231 cells stained with **PS-02** NPs (5 μM) and DiO (10 μM), DiO: excitation light source 488 nm, detection channel 530 ± 20 nm; **PS-02** NPs: excitation light source 559 nm, detection channel 620 ± 20 nm. (b) **PS-02** NP distributions in three different human breast cells, breast cancer cell MDA-MB-231 is **CAIX** high-expression, breast cancer cell MCF-7 is **CAIX** low-expression and normal breast cell COS-7 is **CAIX** low-expression. (c) CLSM imaging of a cell membrane stained by **PS-02** NPs at different times, excitation light source 559 nm, detection channel 620 ± 20 nm, scale bar = 50 μm.

© 2024 The Author(s). Published by the Royal Society of Chemistry

Open Access Article. Published on 18 June 2024. Downloaded on 1/21/2026 10:49:51 PM. This article is licensed under a Creative Commons Attribution-NonCommercial 3.0 Unported Licence.

seen from Fig. 2f and g, the $O_2^{\bullet-}$ generation capacity of **PS-01** NPs has been increased by 16.1 times compared to that of **PS** NPs. This favors the design purpose that electron donor piperazine's effect as an electron-rich environment inclined to the occurrence of ET of the type I process in **PS-01** NPs. However, for **PS-02** NPs, the $O_2^{\bullet-}$ generation amounts decreased a lot to only 0.1 compared to that of **PS-01** NPs, which was consistent with the proposed "ET cage" to turn off the type I process. So, when **CAIX** was added, the boosted $O_2^{\bullet-}$ generation recovered (10.7 times that of **PS** NPs), which meant that the "ET cage" built by the ligand **6-NS** was uncaged by **CAIX**. These results confirmed that the strategy of ET programming through the modification of functionalized groups enabled the regulation of the type I process. In order to identify these different ET processes in **PS-01** NPs and **PS-02** NPs, the long-lived excited state properties of the **PS** NPs, **PS-01** NPs and **PS-02** NPs were studied by transient absorption spectroscopy (Fig. 3). **PS** NPs, **PS-01** NPs, and **PS-02** NPs showed a similar triplet excited state absorption at the 640 nm and 400 nm peaks and ground state depletion at the 565 nm and 465 nm peaks (Fig. 3a–c). The differences mainly lie in the kinetic decay process of the triple excited state of ^{3}(**PS-01**)* that a new rapid decay process with a fitted lifetime $\tau_1 =$ 35.05 ns appeared compared with **PS** NPs and **PS-02** NPs (Fig. 2d–f). It should be assigned to the ET quenching process derived from the modified electron piperazine in **PS-01**. Correspondingly, we did detect the single-electron reduction excited state species (**PS-01**)$^{\bullet-}$ at 420 nm only in **PS-01** NPs but not in **PS** NPs and **PS-02** NPs (Fig. 3g–i).[35,53] This long-lived radical anion species ($\tau_2 =$ 43.96 μs) determined the effective O_2 to $O_2^{\bullet-}$ photosensitization. Furthermore, this disappeared ET quenching process in **PS-02** NPs meant the ET from piperazine was inhibited. And the absence of the intermediate photosensitizer free radical anion resulted in the off state of the type I process in **PS-02** NPs, which was consistent with the significant drop in $O_2^{\bullet-}$ generation. We speculate that in **PS-02** NPs the ligand **6-NS** should form a local cage to block the ET process.

CAIX-integrated tumor cell targeting and type I PDT boosting *in vitro*

In the above, we have confirmed that the functional nanoparticle **NP-02** NPs possessed the ability for **CAIX**-activation for boosted $O_2^{\bullet-}$ generation in solution. Next, we evaluated the type I PDT performance afforded by this merit in living tumor cells. First, the targeting capability of **PS-02** NPs oriented by **CAIX** was verified by confocal laser scanning microscopy (CLSM) imaging. In the **CAIX** high-expressive human breast cancer cell of MDA-MB-231, the distribution of **PS-02** NPs in the cell membrane was observed. And it was further checked by a colocalization experiment with a commercial membrane dye DiO (Fig. 4a). In

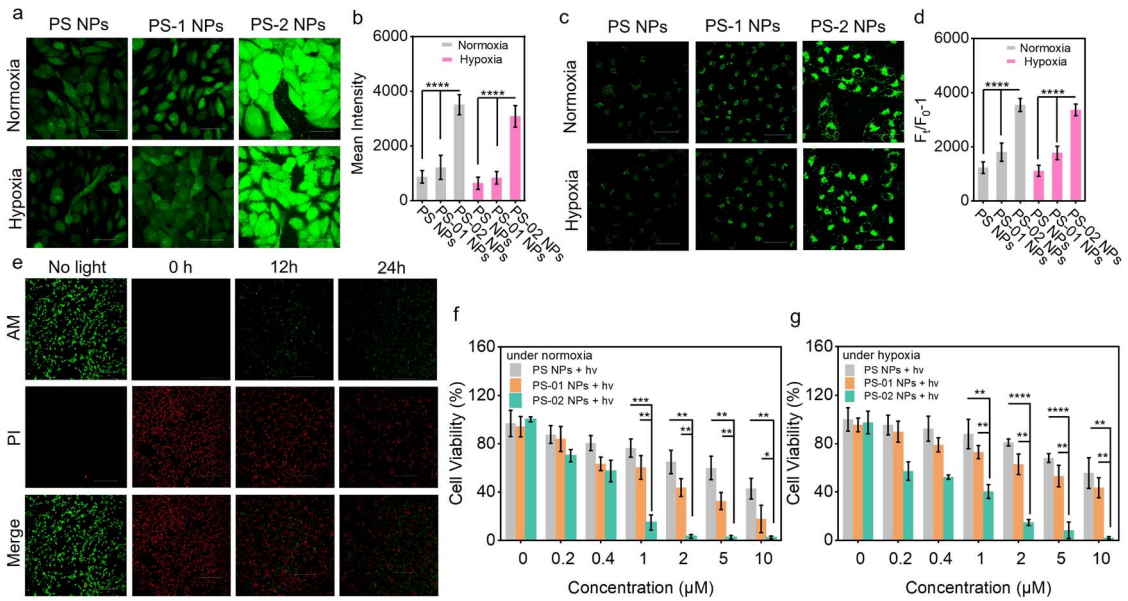

Fig. 5 The ROS amount detection and tumor cell PDT experiment *in vitro*. (a) The ROS production of **PS** NPs, **PS-01** NPs, and **PS-02** NPs (5 μM) in MDA-MB-231 cells under light treatment and detection by DCFH (1 μM). Excitation light source 488 nm, detection channel wavelength = 530 ± 20 nm, scale bar = 50 μm. (b) The histogram of fluorescence intensity of DCFH in (a). (c) The $O_2^{\bullet-}$ production of **PS** NPs, **PS-01** NPs, and **PS-02** NPs (5 μM) under light treatment and detection by DHR 123 (10 μM). Excitation light source 488 nm, detection channel wavelength 530 ± 20 nm, scale bar = 50 μm. (d) The histogram of fluorescence intensity of DHR 123 in (c). (e) CLSM imaging of live and dead cells treated with **PS-02** NPs (5 μM) under light treatment by calcein AM (2 μM)/propidium iodide (PI) (4 μM) staining. After the cells were once stained by **PS-02** NPs, the same light treatment was conducted at 0 h, 12 h, and 24 h, respectively. (Calcein AM: excitation light source 488 nm, detection channel wavelength = 530 ± 20 nm; PI: excitation light source 559 nm, detection channel wavelength = 650 ± 50 nm), scale bar = 300 μm. (f) Relative viabilities of MDA-MB-231 cells treated with different concentrations of **PS** NPs, **PS-01** NPs and **PS-02** NPs under light treatment under normoxic conditions. (g) Relative viabilities of MDA-MB-231 cells treated with different concentrations of **PS** NPs, **PS-01** NPs, and **PS-02** NPs under light treatment under hypoxic conditions (light treatment conditions: irradiation by white light, 20 mW cm^{-2}, 0.5 h). All data in (b), (d) (f) and (g) are presented as mean ± SD. Statistical significance was analyzed by the Student's *t*-test. ****$p < 0.0001$; ***$p < 0.001$; **$p < 0.01$; *$p < 0.05$.

Open Access Article. Published on 18 June 2024. Downloaded on 1/21/2026 10:49:51 PM. This article is licensed under a Creative Commons Attribution-NonCommercial 3.0 Unported Licence.

contrast, under the same conditions, **PS** NPs and **PS-01** NPs with no target ligand modification showed little accumulation in MDA-MB-231 (Fig. S3†). As expected, the accumulation of **PS-02** NPs in the **CAIX** low-expression one such as breast cancer cells of MCF-7 or normal breast cells COS-7 was rather low (Fig. 4b). Meanwhile, **PS-02** NPs could be anchored in MDA-MB-231 cells for as long as 48 h (Fig. 4c). These results supported that the tight **CAIX**-anchoring features enabled **PS-02** NPs to target tumor cells selectively. After confirming the **CAIX**-mediated tumor cell target function in **PS-02** NPs, it is time to check whether **CAIX** could still boost type I photosensitization in living cells. We chose MDA-MB-231 tumor cells treated with **PS-02** NPs as the experiment group and those treated with **PS** NPs and **PS-01** NPs as control groups, separately. The total ROS generation amounts were captured and analyzed with an ROS indicator (DCFH-DA) in CLSM imaging. As shown in Fig. 5a and b, the experimental groups treated by **PS-02** NPs maintained the highest ROS generation amounts compared to **PS** NPs and **PS-01** NPs under both normoxic and hypoxic conditions. Then, the boosted $O_2^{\bullet-}$ producing ability was evaluated again by using the $O_2^{\bullet-}$ indicator (DHR 123) (Fig. 5c and d). The fluorescence imaging indicated that **PS-02** NPs had the best performance of the type I process in the living cells. And the significantly enhanced $O_2^{\bullet-}$ on tumor cells' killing effect was further evaluated by the live/dead cell co-staining assay (Fig. 5e). Obviously, **PS-02** NPs showed pronounced phototoxicity to tumor cells. Owing to the firm anchoring effect of **CAIX**, **PS-02** NPs maintained an excellent tumor cell killing effect even at 24 h after once staining compared with those of **PS** NPs and **PS-01** NPs (Fig. S4†). In order to further elucidate the detailed **CAIX**-assisted PDT process induced by **PS-02** NPs, the time series cell membrane morphology change was monitored by CLSM imaging (Fig. S5†). After light irradiation, lots of bubbles appeared around the plasma membrane and gradually grew out largely into rupture only in 8 min. Next, the phototoxicity of **PS-02** NPs to tumor cells was quantitatively evaluated by the MTT assay. As shown in Fig. 5f and g, **PS-02** NPs exhibited the best tumor cell killing effect compared to **PS** NPs and **PS-01** NPs, and the half maximal inhibitory concentration (IC_{50}) of **PS-02** NPs was as low as 0.34 ± 0.05 μM under normoxic PDT conditions. Under hypoxic PDT conditions, **PS-02** NPs still had a much lower IC_{50} of 0.52 ± 0.15 μM. At the same time, the almost no obvious cell viability change under dark conditions demonstrated all of the three nanoparticles were low biologically toxic (Fig. S6†). All the cellular experiments proved that **PS-02** NPs could not only realize the tumor cell targeting but exert significantly boosted type I PDT even under hypoxia.

Tumor-targeting type I PDT *in vivo*

Furthermore, the selective tumor therapeutic effect of **PS-02** NPs was evaluated in mouse subcutaneous tumor models. Tumor-bearing BAL b/c mice were established and randomly divided into five groups. The group treated with saline with irradiation, **PS-02** NPs without irradiation, **PS** NPs with irradiation, and **PS-01** NPs with irradiation were separately set as control groups, and **PS-02** NPs with irradiation were set as experiment groups.

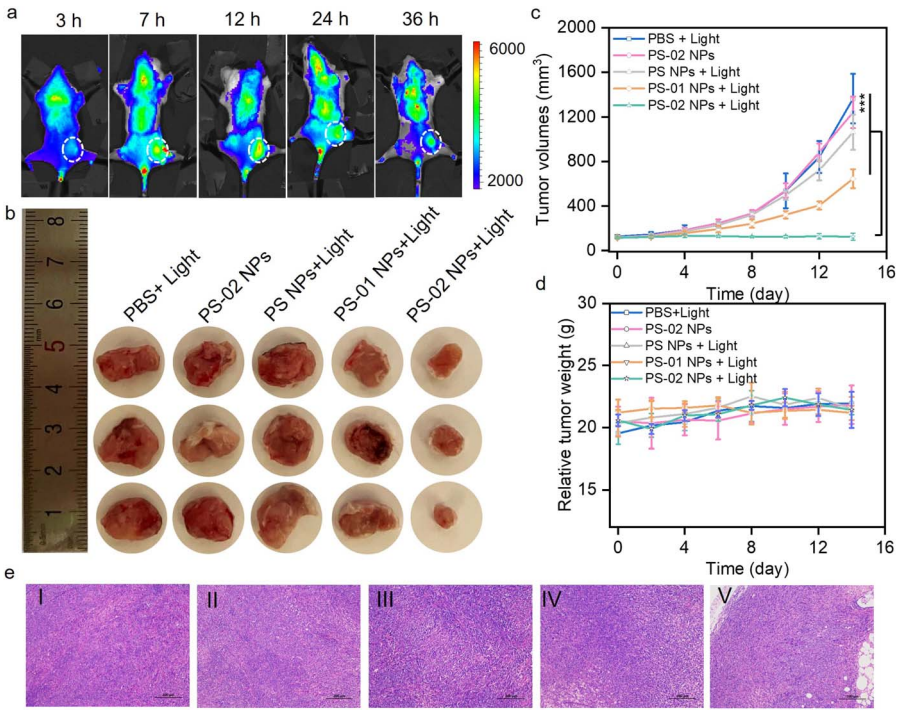

Fig. 6 The evaluation of PDT treatment in tumor-bearing mice. (a) Fluorescence imaging by **PS-02** NPs in tumor tissue. (b) The photographs of *ex vivo* tumors from tumor-bearing mice with different treatment groups. (c) The tumor volume growth curves from tumor-bearing mice with different treatment groups ($n = 3$). (d) The body weight curves of the mice with different treatments ($n = 3$). (e) H&E-stained tumors from BAL b/c mice after different treatments. Scale bar = 100 μm. I: PBS + light, II: **PS-02** NPs, III: **PS** NPs + light, IV: **PS-01** NPs + light and V: **PS-02** NPs + light. All data in (c) and (d) are presented as mean ± SD. Statistical significance was analyzed by the Student's *t*-test. ***$p < 0.001$.

© 2024 The Author(s). Published by the Royal Society of Chemistry

Open Access Article. Published on 18 June 2024. Downloaded on 1/21/2026 10:49:51 PM. This article is licensed under a Creative Commons Attribution-NonCommercial 3.0 Unported Licence.

First, the tumor-selective accumulation of **PS-02** NPs in mice was administrated by way of intravenous injection. From Fig. 6a and S7,† **PS-02** NPs were observed to realize efficient accumulation in tumor areas for as long as 36 h, which provides a suitable window time for tumor treatment. Following the guidance of good tumor fluorescence imaging, we conducted PDT experiments in the tumor region at 12 h and 36 h after drug injection once. As can be seen from Fig. 6b and c, only the group treated with **PS-02** NPs + light exhibited a significant tumor-suppressing efficacy, outperforming the other groups. During this process, all mice did show no noticeable abnormal body weight changes (Fig. 6d). Hematoxylin and eosin (H&E) histological analysis was applied to reveal the necrosis of tumor tissue induced by the PDT of **PS-02** NPs (Fig. 6e). These results consistently suggested that **PS-02** NPs can exert an excellent tumor curative effect in mice. Moreover, no noticeable cell necrosis and inflammation lesions including in the heart, liver, spleen, lungs, and kidneys appeared in H&E staining imaging (Fig. S8†). Collectively, **PS-02** NPs hold impressive therapeutic potential for tumor PDT due to their excellent tumor inhibition efficiency and biocompatibility.

Conclusions

This work introduced a novel and feasible integrated system for the efficient treatment of hypoxic tumors by rationally leveraging the self-assembly and electron transfer programming strategy. In detail, we have developed two functional amphiphile **PS-01** and **PS-02** from TADF-type photosensitizer **PS** by importing an electron-rich group and additionally modifying tumor marker-targeting ligand **6-NS**. These amphiphiles tend to assemble into nanoparticles of **PS** NPs, **PS-01** NPs, and **PS-02** NPs. **PS-01** NPs showed augmented type I photosensitization (16.1 times $O_2^{\bullet-}$ compared to that of **PS** NPs) owing to the local electron-rich environment provided by the electron donor. **PS-02** NPs showed "off state" (0.1 times $O_2^{\bullet-}$ compared to that of **PS** NPs) type I photosensitization, and we inferred that the electron-deficient ligand **6-NS** would work as an "electron transfer cage" to block the ET process in **PS-02** NPs. Consistently, when **PS-02** NPs targeted and tightly bound to the tumor marker **CAIX**, the electron-rich nature of **CAIX** afforded the ability of uncaging the ET effect to boost type I photosensitization (10.7 times $O_2^{\bullet-}$ compared to that of **PS** NPs). So, **PS-02** NPs have integrated their tumor targeting ability with boosted type I photosensitization. It is noteworthy that the significantly improved therapeutic performance of **PS-02** NPs was demonstrated with hypoxic tumor cells and solid tumor tissue in mice. We believe this accessible strategy would rejuvenate the development of more functionalized PSs for practical tumor treatments.

Data availability

The crystal structure data of **CAIX** was deposited at the Protein Data Bank (PDB) with the PDB code 3IAI on the PDB website (**https://www.rcsb.org/**). All experimental supporting data and procedures are available in the ESI.†

Author contributions

Wenlong Chen and Zehui Wang contributed equally to this work and participated in all experimental processes. Gaobo Hong conducted the data curation; Jianju Du, Fengling Song, and Xiaojun Peng provided the conceptualization and supervision. Wenlong Chen, Zehui Wang, and Fengling Song conducted the writing – original draft and review & editing.

Conflicts of interest

There are no conflicts to declare.

Acknowledgements

This work was supported financially by the Guangdong Basic and Applied Basic Research Foundation (2024A1515012493), the National Key Research and Development Program of China (2023YFC3403000), the National Natural Science Foundation of China (22378231) and the Fundamental Research Funds of Shandong University.

Notes and references

1 X. Li, J. F. Lovell, J. Yoon and X. Chen, Clinical development and potential of photothermal and photodynamic therapies for cancer, *Nat. Rev. Clin. Oncol.*, 2020, **17**, 657–674.
2 T. C. Pham, V.-N. Nguyen, Y. Choi, S. Lee and J. Yoon, Recent Strategies to Develop Innovative Photosensitizers for Enhanced Photodynamic Therapy, *Chem. Rev.*, 2021, **121**, 13454–13619.
3 C. Willyard, The innovative therapies that could break the brain-cancer stalemate, *Nature*, 2018, **561**, S59–S61.
4 P. Agostinis, K. Berg, K. A. Cengel, T. H. Foster, A. W. Girotti, S. O. Gollnick, S. M. Hahn, M. R. Hamblin, A. Juzeniene, D. Kessel, M. Korbelik, J. Moan, P. Mroz, D. Nowis, J. Piette, B. C. Wilson and J. Golab, Photodynamic Therapy of Cancer: An Update, *Ca-Cancer J. Clin.*, 2011, **61**, 250–281.
5 J. Nam, S. Son, K. S. Park, W. Zou, L. D. Shea and J. J. Moon, Cancer nanomedicine for combination cancer immunotherapy, *Nat. Rev. Mater.*, 2019, **4**, 398–414.
6 B. M. Vickerman, E. M. Zywot, T. K. Tarrant and D. S. Lawrence, Taking phototherapeutics from concept to clinical launch, *Nat. Rev. Chem*, 2021, **5**, 816–834.
7 R. Liu, Y. Xu, N. Zhang, S. Qu, W. Zeng, R. Li and Z. Dai, *Nanomedicine*, 2023, 99–156, DOI: **10.1007/978-981-16-8984-0_8**, ch. Chapter 8.
8 G. F. Beeghly, A. A. Shimpi, R. N. Riter and C. Fischbach, Measuring and modelling tumour heterogeneity across scales, *Nat. Rev. Bioeng.*, 2023, **1**, 712–730.
9 S. Wilhelm, A. J. Tavares, Q. Dai, S. Ohta, J. Audet, H. F. Dvorak and W. C. W. Chan, Analysis of nanoparticle delivery to tumours, *Nat. Rev. Mater.*, 2016, **1**, 16014.
10 K. Hida, N. Maishi, Y. Sakurai, Y. Hida and H. Harashima, Heterogeneity of tumor endothelial cells and drug delivery, *Adv. Drug Delivery Rev.*, 2016, **99**, 140–147.

© 2024 The Author(s). Published by the Royal Society of Chemistry

Open Access Article. Published on 18 June 2024. Downloaded on 1/21/2026 10:49:51 PM. This article is licensed under a Creative Commons Attribution-NonCommercial 3.0 Unported Licence.

11 M. J. Mitchell, M. M. Billingsley, R. M. Haley, M. E. Wechsler, N. A. Peppas and R. Langer, Engineering precision nanoparticles for drug delivery, *Nat. Rev. Drug Discovery*, 2021, **20**, 101–124.
12 S. K. Singh and R. Singh, Nanotherapy: targeting the tumour microenvironment, *Nat. Rev. Cancer*, 2022, **22**, 258.
13 V. Bhandari, C. Hoey, L. Y. Liu, E. Lalonde, J. Ray, J. Livingstone, R. Lesurf, Y.-J. Shiah, T. Vujcic, X. Huang, S. M. G. Espiritu, L. E. Heisler, F. Yousif, V. Huang, T. N. Yamaguchi, C. Q. Yao, V. Y. Sabelnykova, M. Fraser, M. L. K. Chua, T. van der Kwast, S. K. Liu, P. C. Boutros and R. G. Bristow, Molecular landmarks of tumor hypoxia across cancer types, *Nat. Genet.*, 2019, **51**, 308–318.
14 G. He, Y. Li, M. R. Younis, L.-H. Fu, T. He, S. Lei, J. Lin and P. Huang, Synthetic biology-instructed transdermal microneedle patch for traceable photodynamic therapy, *Nat. Commun.*, 2022, **13**, 6238.
15 X. Liu, S. Viswanadhapalli, S. Kumar, T.-K. Lee, A. Moore, S. Ma, L. Chen, M. Hsieh, M. Li, G. R. Sareddy, K. Parra, E. B. Blatt, T. C. Reese, Y. Zhao, A. Chang, H. Yan, Z. Xu, U. P. Pratap, Z. Liu, C. M. Roggero, Z. Tan, S. T. Weintraub, Y. Peng, R. R. Tekmal, C. L. Arteaga, J. Lippincott-Schwartz, R. K. Vadlamudi, J.-M. Ahn and G. V. Raj, Targeting LIPA independent of its lipase activity is a therapeutic strategy in solid tumors via induction of endoplasmic reticulum stress, *Nat. Cancer*, 2022, **3**, 866–884.
16 M. Srinivasarao and P. S. Low, Ligand-Targeted Drug Delivery, *Chem. Rev.*, 2017, **117**, 12133–12164.
17 A. Vito, N. El-Sayes and K. Mossman, Hypoxia-Driven Immune Escape in the Tumor Microenvironment, *Cells*, 2020, **9**, 992.
18 B. Pucelik, A. Sulek, A. Barzowska and J. M. Dabrowski, Recent advances in strategies for overcoming hypoxia in photodynamic therapy of cancer, *Cancer Lett.*, 2020, **492**, 116–135.
19 D. E. J. G. J. Dolmans, D. Fukumura and R. K. Jain, Photodynamic therapy for cancer, *Nat. Rev. Cancer*, 2003, **3**, 380–387.
20 S. Singh, A. Aggarwal, N. V. Bhupathiraju, G. Arianna, K. Tiwari and C. M. Drain, Glycosylated Porphyrins, Phthalocyanines, and Other Porphyrinoids for Diagnostics and Therapeutics, *Chem. Rev.*, 2015, **115**, 10261–10306.
21 M. Li, J. Xia, R. Tian, J. Wang, J. Fan, J. Du, S. Long, X. Song, J. W. Foley and X. Peng, Near-Infrared Light-Initiated Molecular Superoxide Radical Generator: Rejuvenating Photodynamic Therapy against Hypoxic Tumors, *J. Am. Chem. Soc.*, 2018, **140**, 14851–14859.
22 J. Du, T. Shi, S. Long, P. Chen, W. Sun, J. Fan and X. Peng, Enhanced photodynamic therapy for overcoming tumor hypoxia: From microenvironment regulation to photosensitizer innovation, *Coord. Chem. Rev.*, 2021, **427**, 213604.
23 M. Li, Y. Xu, X. Peng and J. S. Kim, From Low to No O2-Dependent Hypoxia Photodynamic Therapy (hPDT): A New Perspective, *Acc. Chem. Res.*, 2022, **55**, 3253–3264.
24 W. Fan, P. Huang and X. Chen, Overcoming the Achilles' heel of photodynamic therapy, *Chem. Soc. Rev.*, 2016, **45**, 6488–6519.
25 T. C. Pham, V. N. Nguyen, Y. Choi, S. Lee and J. Yoon, Recent Strategies to Develop Innovative Photosensitizers for Enhanced Photodynamic Therapy, *Chem. Rev.*, 2021, **121**, 13454–13619.
26 R. Docampo, S. N. J. Moreno, R. P. A. Muniz, F. S. Cruz and R. P. Mason, Light-Enhanced Free Radical Formation and Trypanocidal Action of Gentian Violet (Crystal Violet), *Science*, 1983, **220**, 1292–1295.
27 L. Yu, Y. Xu, Z. Pu, H. Kang, M. Li, J. L. Sessler and J. S. Kim, Photocatalytic Superoxide Radical Generator that Induces Pyroptosis in Cancer Cells, *J. Am. Chem. Soc.*, 2022, **144**, 11326–11337.
28 Z. Shen, S. Zheng, Y. Fang, G. Zhang, C. Zhu, S. Liu and J. Hu, Overcoming the Oxygen Dilemma in Photoredox Catalysis: Near-Infrared (NIR) Light-Triggered Peroxynitrite Generation for Antibacterial Applications, *Angew. Chem., Int. Ed.*, 2023, **62**, e202219153.
29 K. Chen, P. He, Z. Wang and B. Z. Tang, A Feasible Strategy of Fabricating Type I Photosensitizer for Photodynamic Therapy in Cancer Cells and Pathogens, *ACS Nano*, 2021, **15**, 7735–7743.
30 Y. Wang, J. Liao, Y. Lyu, Q. Guo, Z. Zhu, X. Wu, J. Yu, Q. Wang and W.-H. Zhu, An AIE Photosensitizer with Simultaneous Type I and Type II ROS Generation: Efficient Bacterial Elimination and Hypoxic Tumor Ablation, *Adv. Funct. Mater.*, 2023, **33**, 2301692.
31 D. Chen, Q. Xu, W. Wang, J. Shao, W. Huang and X. Dong, Type I Photosensitizers Revitalizing Photodynamic Oncotherapy, *Small*, 2021, **17**, e2006742.
32 K. X. Teng, W. K. Chen, L. Y. Niu, W. H. Fang, G. Cui and Q. Z. Yang, BODIPY-Based Photodynamic Agents for Exclusively Generating Superoxide Radical over Singlet Oxygen, *Angew. Chem., Int. Ed.*, 2021, **60**, 19912–19920.
33 D. Chen, Z. Wang, H. Dai, X. Lv, Q. Ma, D.-P. Yang, J. Shao, Z. Xu and X. Dong, Boosting $O_2^{\bullet-}$ Photogeneration via Promoting Intersystem-Crossing and Electron-Donating Efficiency of Aza-BODIPY-Based Nanoplatforms for Hypoxic-Tumor Photodynamic Therapy, *Small Methods*, 2020, **4**, 2000013.
34 H. Ding, H. Yu, Y. Dong, R. Tian, G. Huang, D. A. Boothman, B. D. Sumer and J. Gao, Photoactivation switch from type II to type I reactions by electron-rich micelles for improved photodynamic therapy of cancer cells under hypoxia, *J. Controlled Release*, 2011, **156**, 276–280.
35 W. Chen, Z. Wang, M. Tian, G. Hong, Y. Wu, M. Sui, M. Chen, J. An, F. Song and X. Peng, Integration of TADF Photosensitizer as "Electron Pump" and BSA as "Electron Reservoir" for Boosting Type I Photodynamic Therapy, *J. Am. Chem. Soc.*, 2023, **145**, 8130–8140.
36 X. Li, D. Lee, J. D. Huang and J. Yoon, Phthalocyanine-Assembled Nanodots as Photosensitizers for Highly Efficient Type I Photoreactions in Photodynamic Therapy, *Angew. Chem., Int. Ed.*, 2018, **57**, 9885–9890.

© 2024 The Author(s). Published by the Royal Society of Chemistry

Open Access Article. Published on 18 June 2024. Downloaded on 1/21/2026 10:49:51 PM. This article is licensed under a Creative Commons Attribution-NonCommercial 3.0 Unported Licence.

37 D. Schrama, R. A. Reisfeld and J. C. Becker, Antibody targeted drugs as cancer therapeutics, *Nat. Rev. Drug Discovery*, 2006, **5**, 147–159.
38 M. Gao, F. Yu, C. Lv, J. Choo and L. Chen, Fluorescent chemical probes for accurate tumor diagnosis and targeting therapy, *Chem. Soc. Rev.*, 2017, **46**, 2237–2271.
39 D. Pochan and O. Scherman, Introduction: Molecular Self-Assembly, *Chem. Rev.*, 2021, **121**, 13699–13700.
40 Z. Xie, T. Fan, J. An, W. Choi, Y. Duo, Y. Ge, B. Zhang, G. Nie, N. Xie, T. Zheng, Y. Chen, H. Zhang and J. S. Kim, Emerging combination strategies with phototherapy in cancer nanomedicine, *Chem. Soc. Rev.*, 2020, **49**, 8065–8087.
41 X. Q. Xiong, F. L. Song, J. Y. Wang, Y. K. Zhang, Y. Y. Xue, L. L. Sun, N. Jiang, P. Gao, L. Tian and X. J. Peng, Thermally Activated Delayed Fluorescence of Fluorescein Derivative for Time-Resolved and Confocal Fluorescence Imaging, *J. Am. Chem. Soc.*, 2014, **136**, 9590–9597.
42 C. Lomelino and R. McKenna, Carbonic anhydrase inhibitors: a review on the progress of patent literature (2011-2016), *Expert Opin. Ther. Pat.*, 2016, **26**, 947–956.
43 S. Zhang, C. Yang, W. Lu, J. Huang, W. Zhu, H. Li, Y. Xu and X. Qian, A highly selective space-folded photo-induced electron transfer fluorescent probe for carbonic anhydrase isozymes IX and its applications for biological imaging, *Chem. Commun.*, 2011, **47**, 8301–8303.
44 J. H. Kim, P. Verwilst, M. Won, J. Lee, J. L. Sessler, J. Han and J. S. Kim, A Small Molecule Strategy for Targeting Cancer Stem Cells in Hypoxic Microenvironments and Preventing Tumorigenesis, *J. Am. Chem. Soc.*, 2021, **143**, 14115–14124.
45 H. S. Jung, J. Han, H. Shi, S. Koo, H. Singh, H. J. Kim, J. L. Sessler, J. Y. Lee, J. H. Kim and J. S. Kim, Overcoming the Limits of Hypoxia in Photodynamic Therapy: A Carbonic Anhydrase IX-Targeted Approach, *J. Am. Chem. Soc.*, 2017, **139**, 7595–7602.
46 H. S. Jung, S. Koo, M. Won, S. An, H. Park, J. L. Sessler, J. Han and J. S. Kim, Cu(ii)-BODIPY photosensitizer for CAIX overexpressed cancer stem cell therapy, *Chem. Sci.*, 2023, **14**, 1808–1819.
47 J. H. Kim, S. Park, E. Jung, J. Shin, Y. J. Kim, J. Y. Kim, J. L. Sessler, J. H. Seo and J. S. Kim, A dual-action niclosamide-based prodrug that targets cancer stem cells and inhibits TNBC metastasis, *Proc. Natl. Acad. Sci. U.S.A.*, 2023, **120**, e2304081120.
48 D. Lombardo, M. A. Kiselev, S. Magazù and P. Calandra, Amphiphiles Self-Assembly: Basic Concepts and Future Perspectives of Supramolecular Approaches, *Adv. Condens. Matter Phys.*, 2015, **2015**, 1–22.
49 C. Po, A. Y. Tam, K. M. Wong and V. W. Yam, Supramolecular self-assembly of amphiphilic anionic platinum(II) complexes: a correlation between spectroscopic and morphological properties, *J. Am. Chem. Soc.*, 2011, **133**, 12136–12143.
50 E. Feng, Y. Liu, S. Lv, D. Liu, S. Huang, Z. Li and F. Song, Fine-Tuning Cu (II)-Induced Self-Assembly of Hydrophilic Cyanine Dyes for Enhanced Tumor Photothermal Therapy, *Adv. Funct. Mater.*, 2022, **32**, 2209258.
51 H. Wu, F. Chen, C. You, Y. Zhang, B. Sun and Q. Zhu, Smart Porous Core-Shell Cuprous Oxide Nanocatalyst with High Biocompatibility for Acid-Triggered Chemo/Chemodynamic Synergistic Therapy, *Small*, 2020, **16**, e2001805.
52 S. Wang, M. Rong, H. Li, T. Xu, Y. Bu, L. Chen, X. Chen, Z. P. Yu, X. Zhu, Z. Lu and H. Zhou, Unveiling Mechanism of Organic Photogenerator for Hydroxyl Radicals Generation by Molecular Modulation, *Small*, 2022, **18**, e2104857.
53 T. Tachikawa, Y. Kobori, K. Akiyama, A. Katsuki, Y. Usui, U. E. Steiner and S. Tero-Kubota, Solvent effects on the intrinsic enhancement factors of the triplet exciplex generated by photoinduced electron transfer reaction between eosin Y and duroquinone, *Mol. Phys.*, 2002, **100**, 1413–1420.